

---

This is an electronic reprint of the original article.  
This reprint may differ from the original in pagination and typographic detail.

Tiihonen, Armi; Siipola, Virpi; Lahtinen, Katja; Pajari, Heikki; Widsten, Petri; Tamminen, Tarja; Kallio, Tanja; Miettunen, Kati

## Biocarbon from brewery residues as a counter electrode catalyst in dye solar cells

*Published in:*  
Electrochimica Acta

*DOI:*  
[10.1016/j.electacta.2020.137583](https://doi.org/10.1016/j.electacta.2020.137583)

Published: 01/02/2021

*Document Version*  
Peer-reviewed accepted author manuscript, also known as Final accepted manuscript or Post-print

*Published under the following license:*  
CC BY-NC-ND

*Please cite the original version:*  
Tiihonen, A., Siipola, V., Lahtinen, K., Pajari, H., Widsten, P., Tamminen, T., Kallio, T., & Miettunen, K. (2021). Biocarbon from brewery residues as a counter electrode catalyst in dye solar cells. *Electrochimica Acta*, 368, Article 137583. <https://doi.org/10.1016/j.electacta.2020.137583>

---

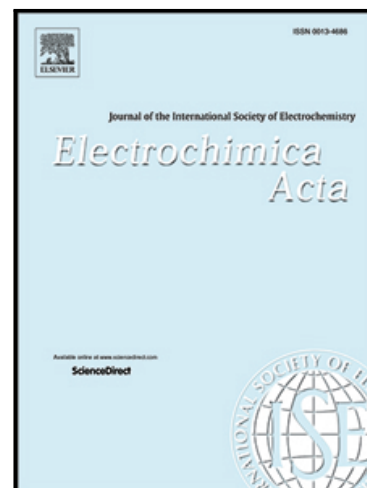
This material is protected by copyright and other intellectual property rights, and duplication or sale of all or part of any of the repository collections is not permitted, except that material may be duplicated by you for your research use or educational purposes in electronic or print form. You must obtain permission for any other use. Electronic or print copies may not be offered, whether for sale or otherwise to anyone who is not an authorised user.

## Journal Pre-proof

Biocarbon from brewery residues as a counter electrode catalyst in dye solar cells

Armi Tiihonen , Virpi Siipola , Katja Lahtinen , Heikki Pajari ,  
Petri Widsten , Tarja Tamminen , Tanja Kallio , Kati Miettunen

PII: S0013-4686(20)31976-9  
DOI: <https://doi.org/10.1016/j.electacta.2020.137583>  
Reference: EA 137583



To appear in: *Electrochimica Acta*

Received date: 10 August 2020  
Revised date: 17 November 2020  
Accepted date: 28 November 2020

Please cite this article as: Armi Tiihonen , Virpi Siipola , Katja Lahtinen , Heikki Pajari ,  
Petri Widsten , Tarja Tamminen , Tanja Kallio , Kati Miettunen , Biocarbon from brewery  
residues as a counter electrode catalyst in dye solar cells, *Electrochimica Acta* (2020), doi:  
<https://doi.org/10.1016/j.electacta.2020.137583>

This is a PDF file of an article that has undergone enhancements after acceptance, such as the addition of a cover page and metadata, and formatting for readability, but it is not yet the definitive version of record. This version will undergo additional copyediting, typesetting and review before it is published in its final form, but we are providing this version to give early visibility of the article. Please note that, during the production process, errors may be discovered which could affect the content, and all legal disclaimers that apply to the journal pertain.

© 2020 Elsevier Ltd. All rights reserved.

Biocarbon from brewery residues as a counter electrode catalyst in dye solar cells

Armi Tiihonen<sup>a,b,1,\*</sup>, Virpi Siipola<sup>c</sup>, Katja Lahtinen<sup>d</sup>, Heikki Pajari<sup>c</sup>, Petri Widsten<sup>c</sup>, Tarja Tamminen<sup>c</sup>, Tanja Kallio<sup>d</sup>, Kati Miettunen<sup>a,e,\*</sup>

<sup>a</sup>Department of Bioproducts and Biosystems, Aalto University, P.O.B. 16300, FI-00076 AALTO, Finland

<sup>b</sup>Department of Mechanical Engineering, Massachusetts Institute of Technology, 77 Massachusetts Ave, Cambridge, MA 02139, United States

<sup>c</sup>VTT Technical Research Centre of Finland Ltd., P.O.Box 1000, FI-02044 VTT, Finland

<sup>d</sup>Department of Chemistry and Materials Science, Aalto University, P.O.B. 16300, FI-00076 AALTO, Finland

<sup>e</sup>Faculty of Science and Engineering, University of Turku, FI-20014 Turku, Finland.

\*Corresponding author. e-mail: [armi.tiihonen@gmail.com](mailto:armi.tiihonen@gmail.com) (Armi Tiihonen). e-mail: [kati.miettunen@utu.fi](mailto:kati.miettunen@utu.fi) (Kati Miettunen).

<sup>1</sup>Present address: Massachusetts Institute of Technology

## Highlights

- Novel activated biocarbon from brewer's spent grain is presented
- Biocarbon counter electrodes investigated in complete dye solar cells
- The first long-term illuminated stability test (3000h) of biocarbon dye solar cells
- Biocarbon suggested to slow down electrolyte degradation in dye solar cells

## Abstract

We explore biocarbon as a low-cost, abundant, and environmentally friendly replacement for Pt in dye solar cells. We introduce a novel biochar based on brewery residues with good performance and stability potential as a counter electrode in complete dye solar cells, and present the first long-term stability test results of a biocarbon in complete dye solar cells. The hydrothermally carbonized and KOH-activated brewer's spent grain (BSG) offers an extremely high surface area for catalytic reactions (2190 m<sup>2</sup>/g). Counter electrodes based on this material provide a promising initial performance (efficiency of

\* Corresponding author. Tel: +358 50 468 3431 and e-mail: [armi.tiihonen@gmail.com](mailto:armi.tiihonen@gmail.com) (Armi Tiihonen). Tel: +358 50 344 1729 and e-mail: [kati.miettunen@utu.fi](mailto:kati.miettunen@utu.fi) (Kati Miettunen).

1. Present address: Massachusetts Institute of Technology

3.6 ± 0.2% for biocarbon solar cells compared to 5.3 ± 0.2 for reference cells with Pt catalyst) with current production and the total resistance of solar cells very close to that of Pt based solar cells. In an extended accelerated aging test, the best biocarbon dye solar cell maintained over 86% of its initial efficiency for 3000 h. Moreover, the biocarbon reduced the degradation via loss of electrolyte charge carriers during aging. Based on these results, the activated BSG biocarbon provides a promising alternative for Pt catalysts.

## Keywords

Biocarbon, dye solar cells, stability, counter electrode

## Introduction

The catalyst in conventional high-performance dye solar cells is Pt, an expensive rare earth metal. Low cost, abundant, and environmentally friendly catalyst layers need to be developed to push dye solar cells towards commercialization. Alternative catalysts that have been investigated include carbon structures or polymers.<sup>1-4</sup> Utilizing a carbon-based electrode instead of a conventional Pt based one, provided that the carbon layer can also double as the conductive layer (i.e. avoiding the conventional transparent oxide layer), has been estimated to reduce the embedded energy of the total device by almost 30 %.<sup>5</sup> Furthermore, recovering Pt from the aged device when it is used as a nanolayer is a major challenge.<sup>6</sup> Thus, utilizing a carbon-based catalyst layer is an environmentally preferred option when considering both the performance and lifecycle of solar cells.

Conventionally, the carbon used in solar applications has been based on fossil sources but complex synthetization has limited manufacturing at scale<sup>7</sup>. Utilizing biocarbon instead of fossil carbon is a step towards environmental friendliness and further cost reductions.<sup>8</sup> Biochars are abundant and renewable,

and they are even suitable for biodegradable devices. Utilizing biochars made from biowaste streams or other inedible, underutilized biomaterial streams has recently attracted attention. Many of the tested materials are derived from forestry, such as wood itself,<sup>9,10</sup> fallen leaves,<sup>9,11,12</sup> fallen pine cone flowers,<sup>13</sup> or recovered paper/carton.<sup>9,12,14</sup> Another common source has been side streams or biowaste from food production such as pumpkin stems,<sup>15</sup> eggshells,<sup>16</sup> mangosteen peels,<sup>17</sup> coconut shells,<sup>18</sup> and fish waste.<sup>19</sup> Also marine plants<sup>20</sup> and even human hair<sup>21,22</sup> have been identified as possible sources.

Biocarbons differ from fossil carbon as materials. Biocarbons feature natural nanostructuring and are likely to have heterogenic bulk and trace metal (e.g. Fe, Ca, K, Mg, or Na)<sup>23,24</sup> compositions depending on the type of plant they are derived from and the soil in which the plant grew. Nanostructuring could be beneficial when biocarbon is applied as a catalyst because it could provide a high active area for catalytic reactions<sup>2,4</sup>. Trace metals could enhance performance initially e.g. by increasing the catalytic activity, but the doping effect might not last<sup>24</sup>. The trace metals could also pose a challenge in terms of long-term stability by promoting new degradative side reactions in other solar cell components<sup>25</sup>. On the other hand, hydrophilic biocarbon could even improve stability by keeping traces of water that can be present in a dye solar cell from the vicinity of the photoelectrode, where degradation reactions involving water can occur.<sup>26</sup> Due to these distinctive features, biocarbons require investigations of their own when they are considered as catalytic layers.

The catalytic performance of biocarbons varies considerably; many biocarbons have shown very low fill factors (~25 %) in current-potential difference (JV) measurements when applied to dye solar cells, but some biocarbons have matched or exceeded the fill factor obtained with the traditional catalyst material Pt<sup>16-18</sup>. Biocarbon from mangosteen peels serves as such an example.<sup>17</sup> Catalytic performance depends on the redox couple used in the electrolyte, for example in the mangosteen peel demonstration the electrolyte was of organic disulfide/thiolate, not the conventional tri-iodide/iodide.<sup>17</sup> In fact, catalysts

other than Pt have often outperformed Pt catalysts with alternative electrolyte redox couples, such as disulfide/thiolate. The existing literature on the design criteria of carbon catalysts for the triiodide reduction reaction is limited<sup>27,28</sup>. Zhao et al. (5) investigated nonmetal-doped graphene as a triiodide reduction catalyst utilizing DFT, concluding that heteroatoms create more active centers for the reaction. They listed multiple promising doping species, including O and N, that are known to create reactive sites for the catalysis of many other reactions, such as oxygen reduction or hydrogen evolution, and have been suggested for iodide reduction<sup>24,29–34</sup>.

In addition to having reactive sites for the intended reaction and having a high surface area, a good catalyst material also maintains the reactive sites. While promising cases of good catalytic performance by biocarbons have been reported, no stability data of a complete dye solar cell with bio-based counter electrode has been reported in spite of the critical role of high stability in reaching low levelized cost of energy over the solar cell lifetime.<sup>35</sup> Stability reports of solar cells with biocarbons remain extremely scarce also for other types of solar cells, such as perovskite solar cells, and have considered only stability under storage conditions.<sup>8,36</sup> Two studies have looked at cycling a counter electrode-counter electrode cell for 100 cycles in cyclic voltammetry to investigate the stability of the catalyst layer.<sup>11,19</sup> Whilst repeated cyclic voltammetry is a good result and a good initial indication of stability, testing the catalyst material stability in a complete solar device and under illumination is still needed to verify its stability in real life use. In many cases, the stability of an individual component and that of a complete device have differed, which is a true concern.<sup>37–39</sup>

In this contribution, we demonstrated a new brewer's spent grain (BSG) based biocarbon for dye solar cells (**Error! Reference source not found.**) and investigated the cells from a stability viewpoint. Samples of BSG were first hydrothermally carbonized and then KOH-activated to obtain excellent surface areas for catalytic reactions, which made the resulting biocarbons (also known as biochar or hydrochar) highly

interesting for solar cell applications. Here, the biocarbon was characterized in terms of its elemental composition (C, H, N, S, O), porosity, and structure. The biocarbon catalyst layers were used as counter electrodes in complete dye solar cells and compared to conventional Pt counter electrodes to investigate the biocarbon's effect on device performance. Furthermore, we examined the stability of this novel biochar electrode in dye solar cells during an accelerated aging test with 1Sun visible light illumination for an extended duration, 3000 h, corresponding to an illumination dose of 3 years in outdoor conditions. Dye and electrolyte degradation were determined after the aging test to investigate which degradation mechanisms were activated in the solar cells.

## Experimental

### 1.1 Preparation of the activated biocarbon

The brewery residues were hydrothermally carbonized prior to the activation procedure. The hydrothermal carbonization was carried out in a 2 L Hastelloy C276 stirred autoclave. The temperature was 260°C for the duration of 360 min after which the carbonized slurry was filtered in a Büchner funnel using qualitative filter paper MN 616 (Macherey-Nagel). The hydrochar was then rinsed using deionized water and dried at 105°C overnight. Further details of the hydrothermal carbonization can be found in Wikberg et al. 2017.<sup>40</sup>

The chemical activation was performed using potassium hydroxide (KOH) with a KOH to biocarbon ratio of 3:1 (m:m). The KOH was dissolved in deionized water and the solution mixed with the biocarbon. Heating was applied to the KOH-biocarbon slurry to ensure proper wetting of the hydrophobic biocarbon material. The heating temperature and time of the impregnation were approximately 80°C and 3h, respectively. After the impregnation, the biocarbon-KOH slurry was dried at 105°C overnight.

For the heat treatment of the impregnated BSG biocarbon, a 115 L batch retort oven was used. The oven was flushed with nitrogen ( $N_2$ ) prior to heating and  $N_2$  was used for the inert atmosphere during the entire heat treatment. The flow rate of  $N_2$  was 5 L/min. The activation temperature was  $800^\circ\text{C}$  and the duration 2 h.

## 1.2 Preparation of the catalyst layer from activated biocarbon

The electrode paste was prepared by mixing the investigated biocarbon, conductive carbon (Timcal C65) and polyvinylidene fluoride (PVDF, Kureha 9300) with the mass ratio of 92:2:6. N-methyl-2-pyrrolidone (NMP, BASF, Life Science) was used as a solvent in the paste. The paste was mixed with a disperser (Dispermat, VMA-Getzmann GMBH-D-51580 Reichshof) at 1000 rpm. After this, the paste was coated with a doctor blade technique on a glass plate divided into  $0.5\text{ cm} \times 1.0\text{ cm}$  sections with transparent tape with a coating thickness of  $10\text{ }\mu\text{m}$ . Finally, the coating was dried overnight in a fume hood, and the tape was removed when the coating had dried. Graphite from Alfa Aesar (325 mesh, 99.9995 %) was used as a reference material.

## 1.3 Preparation of the solar cells

The substrate for both electrodes was fluorine doped tin oxide (FTO) glass with a sheet resistance of  $15\text{ }\Omega/\text{sq}$  (TEC-15, Pilkington). The glass substrates were washed with mild detergent, and then cleaned by sonication (10 min per solution): first in Hellmanex II solution (Hellma Analytics), then in ethanol, and finally in acetone. Prior to deposition of the electrodes, the substrates were cleaned using UV- $O_3$  treatment (UV/Ozone ProCleaner™, Bioforce Nanosciences) for 20 min.

The photoelectrodes were prepared as described in our previous study.<sup>41</sup>  $TiCl_4$  treatment was done before the deposition of the porous  $TiO_2$  layer with screen printing and then again after sintering of that layer. The  $TiO_2$  pastes (18NR-T, 18-NR-OA) were from Dyesol, and for the dyeing we used  $0.3\text{ mM}$  cis-

Bis(isothiocyanato)(2,2'-bipyridyl-4,4'-dicarboxylato)(4,4'-di-nonyl-2'-bipyridyl)ruthenium(II) dye (Z907, from GreatCell) in 1:1 volumetric acetonitrile-tert-butyl alcohol solution.

The biocarbon counter electrodes were kept at 120 °C for 1 h before starting to prepare the solar cells.

The Pt reference counter electrodes were made using 4 µl of 10mM H<sub>2</sub>PtCl<sub>6</sub> in 2-propanol and then heated at 390°C for 15 min as in our earlier study.<sup>41</sup> After heating, the counter electrodes were kept at 120 °C until cell preparation.

The electrolyte used in this study was 0.05 M I<sub>2</sub>, 0.5 M 1-methylbenzimidazole (NMBI), 0.5M 1-propyl-3-methylimidazolium iodide (PMII), and 0.1 M guanidinium thiocyanate (GuSCN) in 3-methoxypropionitrile. The electrolyte solvent, 3-methoxypropionitrile, was purified as described in our earlier study.<sup>26</sup>

The photoelectrode and counter electrode were glued together using thermoplastic (Surlyn, ca. 50µm thick) heated at 120°C. The electrolyte was filled into the device using predrilled holes in the counter electrode. The electrolyte filling holes were sealed using another layer of thermoplastic and a thin cover glass. Copper tapes were attached to both electrodes to serve as electrical contacts and the edge area between the copper and FTO glass was covered with silver paint (Electrolube) to reduce resistance at the connection. The electrical connection was sealed with a layer of epoxy glue.

#### **1.4 Methodology related to characterization of biocarbon**

The activated carbons produced were characterized for their elemental composition (C, H, N, S and O), BET surface area and porosity. The elemental analysis was performed using a Flash 2000 series analyzer (Thermo Scientific, Waltham, MA, USA). The surface area and porosity measurements were performed using Micromeritics 3Flex analyzer (Norcross, GA, USA). The surface area measurements were conducted in isothermal conditions by immersing the sample tubes containing the degassed biocarbons in liquid nitrogen. Small doses of N<sub>2</sub> were added to the sample resulting in isotherms used for the

calculations. A BET (Brunauer-Emmet-Teller) algorithm<sup>42</sup> was used for the specific surface area calculations and the density functional theory (DFT)<sup>43</sup> for the pore size distributions. Scanning electron microscope (SEM) images were taken with Zeiss Sigma equipment.

### **1.5 Measurements related to solar cells**

JV curves were measured using a solar simulator (Pecell) providing 1Sun illumination at a measurement speed of 10 mV/s. In the JV measurements, the solar cells were fitted with black masks (revealing the whole 0.4cm<sup>2</sup> active area of the solar cells) to prevent scattered light from exaggerating the photocurrent values. The photocurrent was analyzed using incident photon to collected electron (IPCE) measurements using a QEX7 spectral analyzer (PV Measurement Inc). The IPCE spectra were measured in DC mode without bias light.

The aging analysis was done according to principles outlined in our previous contribution related to aging studies of dye solar cells.<sup>44</sup> The solar cells were aged using a LED based lamp system (CREE Edge HO240) that provided 1Sun equivalent illumination in the visible light region. The temperature during the aging was 40 °C, and the ambient humidity during the test varied between 10-26%. The solar cells were measured at regular intervals using BioLogic SP-150 potentiostat and Agilent 34980A Multifunction Switch as the multiplexer. Between the measurements, the solar cells were kept in open circuit conditions. Our previous study shows that these types of solar cells degrade almost identically in open circuit and maximum point conditions.<sup>45</sup> The solar cells were photographed periodically to investigate visible changes in the devices; the methodology in photo analysis is described in literature.<sup>46</sup> At the end of the experiment, we repeated the IV, IPCE and EIS measurements in the same way as the initial measurements.

## Results and discussion

### 1.6 Structure and composition of the biocarbon as a material and film

The BSG material was treated by three successive methods: hydrothermal carbonization (producing the precursor biocarbon), heat treatment, and activation treatment. The biocarbons at each stage were analyzed and compared to elucidate the effects of the treatments on the material.

The chemical activation treatment increased the surface area ( $2190 \text{ m}^2/\text{g}$ ) considerably compared to the surface area of the precursor biocarbon ( $5.2 \text{ m}^2/\text{g}$ ) (Table 1), as expected.<sup>23</sup> Heat treatment without chemicals did not affect the surface area significantly. Both methods produced highly microporous carbons. The activation treatment increased the macropore content more than the heat treatment alone. Both the surface area and the pore volume of the activated biocarbon were high compared to the biocarbons listed in a review<sup>24</sup>.

Elemental analysis (C, H, N, S, O) of the precursor biocarbon (Table 1) showed 3.8 and 15 wt-% of nitrogen and oxygen, respectively. The heat treatment without any chemicals retained the content of N but lowered that of oxygen. The activation treatment retained the O content to a higher degree compared to heat treatment but lowered the nitrogen content. The N content after activation was still 37 % of the original amount. The N and O species are of particular interest because they could enhance the catalytic activity of biocarbon for triiodide reduction as discussed in Introduction.

The analysis of active sites was continued by FTIR. The FTIR spectra (**Error! Reference source not found.**) present the differences in the surface activity between the three stages of treated biocarbons. The activated biocarbon has a higher surface activity compared to heat treated biocarbon. The precursor biocarbon has two alkyl peaks at  $2918$  and  $2849 \text{ cm}^{-1}$ , which have been associated with hydrophobicity.<sup>47</sup> These peaks disappear after the heat and activation treatments. The biocarbon has

peaks at 1699, 1588, 1454, 1204 and 1059  $\text{cm}^{-1}$  that are assigned to carboxyl C=O stretching, aromatic C=C stretching, C-H deformation in lignin and carbohydrates, C-O stretching in lignin and xylan, and C-O stretching of carboxylic acid, ester, and ether groups, respectively.<sup>47-49</sup> The heat treated biocarbon shows only slight activity in the carboxylic acid, ester and ether area. The activated biocarbon retained oxygen related activity slightly better at the carboxyl region at 1700  $\text{cm}^{-1}$  and at the carboxylic acid, ester and ether region at 1096-1033  $\text{cm}^{-1}$ . This aligns with the elemental compositions (Table 1).

The characterizations show that after the final stage of treatments, the biocarbon showed high nitrogen and oxygen contents, a high surface area, and low hydrophobicity. These properties suggest that the material has potential as a catalyst material as discussed in Introduction. The activated biocarbon was fabricated into a paste and blade coated on top of conductive glass substrates to prepare counter electrodes for dye solar cells. The highly porous structure of the counter electrodes made using the biocarbon is shown in **Error! Reference source not found.**. The appearance of the counter electrodes was almost fluffy (thickness of the films was on average 28 $\mu\text{m}$ , see ESI for individual film thicknesses). It is noteworthy that the resulting counter electrodes, while resistant to pressure from the top, flaked rather easily if exposed to shear. This property increased variation in the initial performance and stability behavior of the assembled biocarbon solar cells, and could possibly be reduced by interface optimization, such as coating in two stages with different amounts of solvent in the paste.<sup>8</sup>

### **1.7 Efficiency and stability performance of solar cells with biocarbon**

The biocarbon material was applied as counter electrodes (92 m-% biocarbon with 2 w-% of conductive carbon and 6% of polyvinylidene fluoride to improve mechanical and conductive properties of the electrode) in complete dye solar cells, characterized before and after an extended 3000h aging test, and compared with reference devices with a Pt counter electrode. To maintain the comparability between

the reference and biocarbon solar cells, both cell types were kept exactly similar apart from the counter electrodes. Not all the device components can be optimized for both cell types simultaneously due to differences in e.g. energy levels of the counter electrodes and indirect effects on electrolyte (as shown in more detail later). We chose to maintain a structure as close to our standard reference devices as possible to avoid producing false positive results on the new material (the only difference being thicker 50 $\mu\text{m}$  spacer film to allow space for the thick biocarbon counter electrode). This choice means that while the detected differences between the two solar cells types in this study can be solely attributed to the differing counter electrodes, the efficiency of biocarbon dye solar cells is not fully optimized.

JV tests (**Error! Reference source not found.**, Table 2) show that reference, Pt, and biocarbon solar cells had average efficiencies of 5.3% and 3.6%, respectively. This is an expected result for the relatively large-area (0.4 $\text{cm}^2$  active area) device geometry designed to prevent electrolyte leakages during the long-term aging test with a thicker spacer layer. The solar cells with the biocarbon mostly performed comparably to Pt cells, but the biocarbon devices had a decreased open circuit voltage ( $V_{oc}$ ). Due to biocarbon electrode preparation being a less established process than the reference electrode preparation, there is more variation in the performance of biocarbon solar cells than Pt cells. Specifically, the highest  $V_{oc}$  are given by the thinnest counter electrode layers in this device group (see ESI), which suggest further optimization could increase performance. The observed differences in fill factor  $FF$  and efficiency  $\eta$  between the two cell types are in this case also mainly caused by the difference in  $V_{oc}$ .

The slope of the JV curve ( $R_s$  in Table 2) relates to the internal resistances and includes the potential difference in the catalytic performance of the devices (that is expectedly the main difference in these two types of devices). Thus, the similarity of the slopes between the device types indicates biocarbons giving a good catalytic performance similar to that of the reference Pt. In a literature study

characterizing biocarbons from various sources, many biocarbons severely compromised device performance, resulting in  $FF$  factors in the order of 25%.<sup>9</sup> Biocarbons in this large previous study showed a reduced slope of the IV curve near  $V_{oc}$ , indicating that a decreased  $FF$  was the reason for their lower catalytic performance compared to Pt (unlike here).<sup>9</sup> From that perspective the results gained here with biocarbon are highly promising.

The changes in  $FF$  arising from internal resistances could be divided into three parts; series, electrolyte diffusion, and counter electrode / electrolyte interface resistances with electrochemical impedance spectroscopy. The analysis is not possible in this case because the porous biocarbon counter electrodes have a slow charge transfer. The time constant related to charge transfer at the counter electrode / electrolyte interface with carbon catalyst overlaps with the time constant related to charge transfer at the photoelectrode/electrolyte interface.<sup>50</sup> Thus, these two constants cannot be reliably separated (example data shown in ESI). The analysis is further complicated by the photoelectrode/electrolyte interfacial resistance that is dependent on the potential difference. Since the devices with Pt and biocarbon have completely different  $V_{oc}$ , we cannot assume equal resistances over their photoelectrode/electrolyte interfaces and deduce the resistance of the biocarbon electrode.

The devices were exposed to a very long (3000 h) aging test under visible light. Table 2 shows that the two solar cell types had a similar difference in their performance after the aging test. During the aging in both solar cell types, the short circuit current increased (about  $1\text{mA}/\text{cm}^2$ ) while  $V_{oc}$  decreased in both devices by about 100 mV. In this testing both Pt and carbon solar cells had an average decrease in overall efficiency of approximately 10% per 1000 h, which is generally considered a good result. It is notable that the most stable biocarbon device maintained 86%, 101%, 89%, and 95% of its initial  $\eta$ ,  $J_{sc}$ ,  $V_{oc}$ , and  $FF$ , respectively, during the 3000h aging test (see ESI for individual device data). This demonstrates that biocarbon devices have good stability potential once the adhesion of the biocarbon

to the substrate, that is the suspected main source of variation in stability statistics, is optimized. It may be that the biocarbon would give its best performance as a component of a carbon composite counter electrode. In literature such composite structures have given excellent performance and mechanical stability.<sup>50,51</sup> Here we wanted to focus on the biocarbon itself and thus an electrode structure that would require a minimal number of other components was chosen.

In addition to the JV characteristics presented above, measured in a very accurate solar simulator, coarser *in-situ* aging test data is presented in **Error! Reference source not found.** to reveal the differing behavior of the cells during the aging test. Pt devices showed a clear initial efficiency improvement during the first 100 h of testing, and then started to slowly decline in performance. The biocarbon devices had more variation in the test results. In general, they did not show any initial efficiency improvement but six of the eight devices experienced a period of faster *FF* degradation during the initial 500 h, after which the change slowed down. The two devices lacking this initial deterioration in *FF* were the most stable devices at the end of the aging test and both maintained over 80% of their initial efficiency, whereas the other six cells lost on average one third of their initial efficiency (see ESI for individual device data from solar simulator JV tests). Therefore, avoiding this initial failure, possibly caused by fragility of the biocarbon film, is critical for further improving device stability.

### **1.8 Improvement of quantum efficiency in dye solar cells with biocarbon**

We proceeded to investigate whether biocarbon electrodes have an effect on photoelectrode operation by measuring the incident photon to collected electron (IPCE) efficiency of the solar cells. We measured IPCE without bias light at low light intensity, therefore current limiting factors such as electrolyte diffusion were not expected to affect the measurement result. **Error! Reference source not found.**a-b shows IPCE for the devices in their initial state. The biocarbon devices had on average 12% higher IPCE than those with a Pt counter electrode. After the aging, the biocarbon solar cells continued to deliver

higher IPCE compared to Pt and the difference in the peak IPCE values was similar in the beginning and at the end of the experiment (**Error! Reference source not found.c-d**).

An interesting question is where the higher IPCE in the biocarbon came from. When normalizing the IPCE data, the shapes of the IPCE spectra of both device types are similar, which shows the improvement in biocarbon cells compared to Pt is independent on wavelength. Therefore, the difference is likely related to injection efficiency instead of light harvesting or collection efficiencies which both tend to depend on wavelength<sup>52</sup>. Injection from the excited dye to TiO<sub>2</sub> is affected by surface charges of TiO<sub>2</sub>. Since both solar cell types have exactly similar photoelectrodes, the improved injection efficiency likely relates to biocarbon affecting electrolyte composition which in turn alters TiO<sub>2</sub> surface charges. This can be related to the lower  $V_{oc}$  (determined by the difference between the Fermi level of TiO<sub>2</sub> in the photoelectrode and redox level of the electrolyte) of biocarbon devices observed in the JV analysis earlier. The mechanism could involve the biocarbon absorbing harmful contaminants from the electrolyte (e.g., water since biocarbon has a low hydrophobicity, see FTIR analysis). If the biocarbon gave a higher IPCE due to its protective nature, the fact that the difference in the IPCE remained similar during the aging suggests that this protection towards photoelectrode mainly occurred at the initial state and did not change during aging. That further suggests that the biocarbon could have prevented early degradation due to contaminants that were present already during device assembly.

$J_{sc}$  for Pt cells predicted on the IPCE measurements was  $10.9 \pm 0.4 \text{ mA/cm}^2$ , which corresponds to  $J_{sc}$  actually measured under 1Sun (Table 2:  $10.6 \pm 0.3 \text{ mA/cm}^2$ ). For the biocarbon devices, the measured 1Sun  $J_{sc}$  (Table 2:  $10.6 \pm 0.5 \text{ mA/cm}^2$ ) was 12% lower than the value predicted by the IPCE measurements ( $12.1 \pm 0.2 \text{ mA/cm}^2$ ). A similar discrepancy between the measured and predicted  $J_{sc}$  of Pt solar cells also occurred at the end of the experiment. Since the solar cells had exactly similar photoelectrodes, we regard the likely source to be the different optics in these two configurations that

may have caused the Pt devices to slightly overperform in the JV measurements. The biocarbon electrode is black and larger than the photoelectrodes, preventing back reflection of stray light efficiently, whereas Pt electrodes are highly transparent, allowing back reflection. In the IPCE measurement, the light beam was smaller than the photoelectrode inclined to the electrode surface, and such edge effects did not occur. As a note, the edge effects are one of the reasons why solar cells tend to lose some of their measured efficiency while being upscaled into large area solar cells. The lack of the edge effects in biocarbon devices suggests they can maintain their efficiency value better than traditional Pt devices if upscaled.

### **1.9 Improvement of biocarbon electrolyte stability based on limiting current density analysis**

The output current of a typical dye solar cell increases by increasing light intensity until the surface concentration of tri-iodide at the counter electrode drops due to insufficient mass transport from the photoelectrode to the counter electrode. The maximum current level is called limiting current and depends on the concentration and diffusion coefficients of the redox couple, the distance between the electrodes, and the electrode area.<sup>52</sup> Therefore, investigating the photocurrent of a dye solar cell as a function of light intensity provides a method to investigate electrolyte degradation. Loss of charge carriers, which lowers the limiting current and is visible as decreased  $J_{SC}$  as a function of light intensity, was a common major degradation route for dye solar cells in our previous studies.<sup>45,53,54</sup> **Error!**

**Reference source not found.**a-b shows that Pt and biocarbon solar cells gave initially similar  $J_{SC}$  as a function of intensity. This suggests introducing biocarbon did not lead to strong, immediate reactions depleting charge carriers, which could have been possible e.g. via corroding trace metals in biocarbon material. After the 3000h aging test (**Error! Reference source not found.**a-b), the biocarbon cells

maintained a similar or improved response, while the Pt group showed clearly suppressed  $J_{sc}$  at all light intensities above 1Sun. The difference in the photocurrent vs light intensity response of the two cell groups is further illustrated in **Error! Reference source not found.c** in which an improved response produced values larger than 1. The result suggests that charge transport in the biocarbon devices remained stable, whereas the Pt devices suffered from electrolyte degradation that did not yet affect performance at 1Sun intensity but was very close to start doing that. Therefore, biocarbon seems to provide protection from charge carrier depletion that is a major degradation mechanism in dye solar cells.<sup>26</sup> We hypothesize based on low hydrophobicity of biocarbon (see FTIR analysis of biocarbon) that the protection could arise from biocarbon drawing remnants of water from the electrolyte, thus slowing down electrolyte bleaching reactions involving water.<sup>26</sup>

## Conclusions

This study maps the potential of biocarbon as a counter electrode material for dye solar cells, with specific focus on stability effects that remain very scarcely studied in literature. Concerns on the viability of these biomaterials include particularly the existence of metal impurities in the material, potentially causing degradation in the short or long term, as well as suboptimal catalytic performance.

We demonstrated a new potential material in this study: hydrothermally carbonized brewer's spent grain exposed to thermal and chemical activation treatments had an excellent active area (2190 m<sup>2</sup>/g) for catalytic reactions. The material was tested in complete dye solar cells. To maintain the comparability between the reference solar cells with Pt counter electrodes, both solar cells types were similar apart from their counter electrodes. Therefore, the performance of the biocarbon devices was not fully optimized in this study, leading to a lower initial efficiency compared to the Pt devices, but

delivered a similar slope of the JV curve, indicating good catalytic activity. We exposed solar cells to a 3000h-extended accelerated aging test under visible light illumination. During the aging test, the biocarbon solar cells suffered from a large variation in performance, which we suspect to be caused mainly by mechanical and/or adherence issues of the biocarbon counter electrodes that requires further optimization of the blade coating paste. However, the most stable biocarbon device maintained 86% of its initial efficiency during this ultra-long test, corresponding to 3 years of illumination outdoors, which is a very promising stability result.

Our biocarbon counter electrodes suffered from a lower  $V_{oc}$  compared to the reference solar cells with Pt. This is attributed to layer incompatibility but we expect it could be improved by optimizing the full solar cell structure. The biocarbon did not have any adverse effects on the photocurrent production based on JV measurements of fresh devices and during an aging test. The quantum efficiency of biocarbon was even higher than that of Pt. Moreover, biocarbon electrodes protected solar cells from a common major degradation mechanism of dye solar cells during the degradation test, namely loss of electrolyte charge carriers (detected as a decreased limiting current). These findings suggest that the metal impurities in the biocarbon do not have an adverse effect on the operation of a dye solar cell causing e.g. photoelectrode or electrolyte degradation in the short or long term. On the contrary, our results demonstrate that biocarbon in dye solar cell counter electrodes leads to improved electrolyte protection. This could be linked to the low hydrophobicity of the material adsorbing water traces causing degradation in a dye solar cell.

The material investigated here, activated biocarbon prepared from brewer's spent grain, showed potential as dye solar cell counter electrode material once exposed to an extensive full-cell engineering optimization process. The results demonstrate the potential of biocarbon materials especially for

improving the long-term stability of dye solar cells, and we hope they also encourage future research in this and possibly other emerging photovoltaic fields.

mmc1.docx

## Declaration of Competing Interest

None.

## Acknowledgements

This work was a part of the Academy of Finland's Flagship Programme under Projects No. 318890 and 318891 (Competence Center for Materials Bioeconomy, FinnCERES). Armi Tiihonen thanks also Alfred Kordelin Foundation and Svenska Tekniska Vetenskapsakademien i Finland. Kati Miettunen is grateful for the Academy Fellowship funded by Academy of Finland (grants No. 318557 and 320100). We acknowledge the provision of facilities and technical support (SEM imaging) by Aalto University at OtaNano - Nanomicroscopy Center (Aalto-NMC).

## Appendix

Appendix is submitted as a supplementary document.

## References

- (1) Hashmi, G.; Miettunen, K.; Peltola, T.; Halme, J.; Asghar, I.; Aitola, K.; Toivola, M.; Lund, P. Review of Materials and Manufacturing Options for Large Area Flexible Dye Solar Cells. *Renew. Sustain. Energy Rev.* **2011**, *15* (8), 3717–3732. <https://doi.org/10.1016/j.rser.2011.06.004>.
- (2) Wu, M.; Lin, X.; Wang, T.; Qiu, J.; Ma, T. Low-Cost Dye-Sensitized Solar Cell Based on Nine Kinds of Carbon Counter Electrodes. *Energy Environ. Sci.* **2011**, *4* (6), 2308. <https://doi.org/10.1039/c1ee01059j>.
- (3) Brennan, L. J.; Byrne, M. T.; Bari, M.; Gun'ko, Y. K. Carbon Nanomaterials for Dye-Sensitized Solar Cell Applications: A Bright Future. *Adv. Energy Mater.* **2011**, *1* (4), 472–485. <https://doi.org/10.1002/aenm.201100136>.
- (4) Chen, M.; Shao, L.-L. Review on the Recent Progress of Carbon Counter Electrodes for Dye-Sensitized Solar Cells. *Chem. Eng. J.* **2016**, *304*, 629–645. <https://doi.org/10.1016/j.cej.2016.07.001>.
- (5) Parisi, M. L.; Maranghi, S.; Basosi, R. The Evolution of the Dye Sensitized Solar Cells from Grätzel Prototype to Up-Scaled Solar Applications: A Life Cycle Assessment Approach. *Renew. Sustain. Energy Rev.* **2014**, *39*, 124–138. <https://doi.org/10.1016/j.rser.2014.07.079>.
- (6) Reijnders, L. Design Issues for Improved Environmental Performance of Dye-Sensitized and Organic Nanoparticulate Solar Cells. *J. Clean. Prod.* **2010**, *18* (4), 307–312. <https://doi.org/10.1016/j.jclepro.2009.10.021>.
- (7) Wang, J.; Nie, P.; Ding, B.; Dong, S.; Hao, X.; Dou, H.; Zhang, X. Biomass Derived Carbon for Energy Storage Devices. *J. Mater. Chem. A* **2017**, *5* (6), 2411–2428. <https://doi.org/10.1039/c6ta08742f>.

- (8) Gao, L.; Zhou, Y.; Meng, F.; Li, Y.; Liu, A.; Li, Y.; Zhang, C.; Fan, M.; Wei, G.; Ma, T. Several Economical and Eco-Friendly Bio-Carbon Electrodes for Highly Efficient Perovskite Solar Cells. *Carbon N. Y.* **2020**, *162*, 267–272. <https://doi.org/10.1016/j.carbon.2020.02.049>.
- (9) Xu, S.; Liu, C.; Wiezorek, J. 20 Renewable Biowastes Derived Carbon Materials as Green Counter Electrodes for Dye-Sensitized Solar Cells. *Mater. Chem. Phys.* **2018**, *204*, 294–304. <https://doi.org/10.1016/j.matchemphys.2017.10.056>.
- (10) Jiang, Q. W.; Li, G. R.; Wang, F.; Gao, X. P. Highly Ordered Mesoporous Carbon Arrays from Natural Wood Materials as Counter Electrode for Dye-Sensitized Solar Cells. *Electrochem. commun.* **2010**, *12* (7), 924–927. <https://doi.org/10.1016/j.elecom.2010.04.022>.
- (11) Cha, S. M.; Nagaraju, G.; Sekhar, S. C.; Bharat, L. K.; Yu, J. S. Fallen Leaves Derived Honeycomb-like Porous Carbon as a Metal-Free and Low-Cost Counter Electrode for Dye-Sensitized Solar Cells with Excellent Tri-Iodide Reduction. *J. Colloid Interface Sci.* **2018**, *513*, 843–851. <https://doi.org/10.1016/j.jcis.2017.11.080>.
- (12) Xu, S. One-Step Fabrication of Carbon Fiber Derived from Waste Paper and Its Application for Catalyzing Tri-Iodide Reduction. *IOP Conf. Ser. Earth Environ. Sci.* **2017**, *52*, 012014. <https://doi.org/10.1088/1742-6596/52/1/012014>.
- (13) Nagaraju, G.; Lim, J. H.; Cha, S. M.; Yu, J. S. Three-Dimensional Activated Porous Carbon with Meso/Macropore Structures Derived from Fallen Pine Cone Flowers: A Low-Cost Counter Electrode Material in Dye-Sensitized Solar Cells. *J. Alloys Compd.* **2017**, *693*, 1297–1304. <https://doi.org/10.1016/j.jallcom.2016.10.015>.
- (14) Zhang, Y.; Yun, S.; Wang, Z.; Zhang, Y.; Wang, C.; Arshad, A.; Han, F.; Si, Y.; Fang, W. Highly Efficient Bio-Based Porous Carbon Hybridized with Tungsten Carbide as Counter Electrode for

Dye-Sensitized Solar Cell. *Ceram. Int.* **2020**, *46* (10), 15812–15821.

<https://doi.org/10.1016/j.ceramint.2020.03.128>.

- (15) Madhu, R.; Veeramani, V.; Chen, S.-M.; Palanisamy, J.; Ezhil Vilian, A. T. Pumpkin Stem-Derived Activated Carbons as Counter Electrodes for Dye-Sensitized Solar Cells. *RSC Adv.* **2014**, *4* (109), 63917–63921. <https://doi.org/10.1039/C4RA12585A>.
- (16) Wang, C.-L.; Liao, J.-Y.; Chung, S.-H.; Manthiram, A. Carbonized Eggshell Membranes as a Natural and Abundant Counter Electrode for Efficient Dye-Sensitized Solar Cells. *Adv. Energy Mater.* **2015**, *5* (6), 1401524. <https://doi.org/10.1002/aenm.201401524>.
- (17) Maiaugree, W.; Lowpa, S.; Towannang, M.; Rutphonsan, P.; Tangtrakarn, A.; Pimanpang, S.; Maiaugree, P.; Ratchapolthavisin, N.; Sang-aroon, W.; Jarernboon, W.; Amornkitbamrung, V. A Dye Sensitized Solar Cell Using Natural Counter Electrode and Natural Dye Derived from Mangosteen Peel Waste. *Sci. Rep.* **2015**, *5* (1), 15230. <https://doi.org/10.1038/srep15230>.
- (18) Kumarasinghe, K. D. M. S. P. K.; Kumara, G. R. A.; Rajapakse, R. M. G.; Liyanage, D. N.; Tennakone, K. Activated Coconut Shell Charcoal Based Counter Electrode for Dye-Sensitized Solar Cells. *Org. Electron.* **2019**, *71*, 93–97. <https://doi.org/10.1016/j.orgel.2019.05.009>.
- (19) Ma, P.; Lu, W.; Yan, X.; Li, W.; Li, L.; Fang, Y.; Yin, X.; Liu, Z.; Lin, Y. Heteroatom Tri-Doped Porous Carbon Derived from Waste Biomass as Pt-Free Counter Electrode in Dye-Sensitized Solar Cells. *RSC Adv.* **2018**, *8* (33), 18427–18433. <https://doi.org/10.1039/C8RA02575D>.
- (20) Wang, L.; Shi, Y.; Bai, X.; Xing, Y.; Zhang, H.; Wang, L.; Guo, W.; Wang, N.; Ma, T.; Grätzel, M. From Marine Plants to Photovoltaic Devices. *Energy Environ. Sci.* **2014**, *7* (1), 343–346. <https://doi.org/10.1039/C3EE42767F>.
- (21) Sahasrabudhe, A.; Kapri, S.; Bhattacharyya, S. Graphitic Porous Carbon Derived from Human Hair

- as 'Green' Counter Electrode in Quantum Dot Sensitized Solar Cells. *Carbon N. Y.* **2016**, *107*, 395–404. <https://doi.org/10.1016/j.carbon.2016.06.015>.
- (22) Moolsarn, K.; Tangtrakarn, A.; Pimsawat, A.; Duangsa, K.; Mongkolkachit, C.; Maiaugree, W.; Amornkitbamrung, V. A Dye-Sensitized Solar Cell Using a Composite of PEDOT:PSS and Carbon Derived from Human Hair for a Counter Electrode. *Int. J. Photoenergy* **2017**, *2017*, 1–11. <https://doi.org/10.1155/2017/1064868>.
- (23) Xiong, X.; Yu, I. K. M.; Cao, L.; Tsang, D. C. W.; Zhang, S.; Ok, Y. S. A Review of Biochar-Based Catalysts for Chemical Synthesis, Biofuel Production, and Pollution Control. *Bioresour. Technol.* **2017**, *246*, 254–270. <https://doi.org/10.1016/j.biortech.2017.06.163>.
- (24) Borghei, M.; Lehtonen, J.; Liu, L.; Rojas, O. J. Advanced Biomass-Derived Electrocatalysts for the Oxygen Reduction Reaction. *Advanced Materials*. Wiley-VCH Verlag June 13, 2018. <https://doi.org/10.1002/adma.201703691>.
- (25) Miettunen, K.; Asghar, I.; Ruan, X.; Halme, J.; Saukkonen, T.; Lund, P. Stabilization of Metal Counter Electrodes for Dye Solar Cells. *J. Electroanal. Chem.* **2011**, *653* (1–2), 93–99. <https://doi.org/10.1016/j.jelechem.2010.12.022>.
- (26) Tiihonen, A.; Miettunen, K.; Rendon, S.; Mavrynsky, D.; Halme, J.; Leino, R.; Lund, P. The Effect of Electrolyte Purification on the Performance and Long-Term Stability of Dye-Sensitized Solar Cells. *J. Electrochem. Soc.* **2015**, *162* (9). <https://doi.org/10.1149/2.0671509jes>.
- (27) Zhang, L.; Lin, C.; Zhang, D.; Gong, L.; Zhu, Y.; Zhao, Z.; Xu, Q.; Li, H.; Xia, Z. Guiding Principles for Designing Highly Efficient Metal-Free Carbon Catalysts. *Adv. Mater.* **2019**, *31* (13), 1805252. <https://doi.org/10.1002/adma.201805252>.
- (28) Zhao, Z.; Lin, C. Y.; Tang, J.; Xia, Z. Catalytic Mechanism and Design Principles for Heteroatom-

Doped Graphene Catalysts in Dye-Sensitized Solar Cells. *Nano Energy* **2018**, *49*, 193–199.

<https://doi.org/10.1016/j.nanoen.2018.04.053>.

- (29) Silva, R.; Voiry, D.; Chhowalla, M.; Asefa, T. Efficient Metal-Free Electrocatalysts for Oxygen Reduction: Polyaniline-Derived N- and O-Doped Mesoporous Carbons. *J. Am. Chem. Soc.* **2013**, *135* (21), 7823–7826. <https://doi.org/10.1021/ja402450a>.
- (30) Roy-Mayhew, J. D.; Bozym, D. J.; Punckt, C.; Aksay, I. A. Functionalized Graphene as a Catalytic Counter Electrode in Dye-Sensitized Solar Cells. *ACS Nano* **2010**, *4* (10), 6203–6211. <https://doi.org/10.1021/nn1016428>.
- (31) Tuomi, S.; Pakkanen, O. J.; Borghei, M.; Kronberg, R.; Sainio, J.; Kauppinen, E. I.; Nasibulin, A. G.; Laasonen, K.; Kallio, T. Experimental and Computational Investigation of Hydrogen Evolution Reaction Mechanism on Nitrogen Functionalized Carbon Nanotubes. *ChemCatChem* **2018**, *10* (17), 3872–3882. <https://doi.org/10.1002/cctc.201800479>.
- (32) Rajala, T.; Kronberg, R.; Backhouse, R.; Buan, M. E. M.; Tripathi, M.; Zitolo, A.; Jiang, H.; Laasonen, K.; Susi, T.; Jaouen, F.; Kallio, T. A Platinum Nanowire Electrocatalyst on Single-Walled Carbon Nanotubes to Drive Hydrogen Evolution. *Appl. Catal. B Environ.* **2020**, *265*, 118582. <https://doi.org/10.1016/j.apcatb.2019.118582>.
- (33) Ju, M. J.; Jeon, I.-Y.; Lim, K.; Kim, J. C.; Choi, H.-J.; Choi, I. T.; Eom, Y. K.; Kwon, Y. J.; Ko, J.; Lee, J.-J.; Baek, J.-B.; Kim, H. K. Edge-Carboxylated Graphene Nanoplatelets as Oxygen-Rich Metal-Free Cathodes for Organic Dye-Sensitized Solar Cells. *Energy Environ. Sci.* **2014**, *7* (3), 1044–1052. <https://doi.org/10.1039/C3EE43732A>.
- (34) Hou, S.; Cai, X.; Wu, H.; Yu, X.; Peng, M.; Yan, K.; Zou, D. Nitrogen-Doped Graphene for Dye-Sensitized Solar Cells and the Role of Nitrogen States in Triiodide Reduction. *Energy Environ. Sci.*

- 2013**, *6* (11), 3356–3362. <https://doi.org/10.1039/C3EE42516A>.
- (35) Peters, I. M.; Rodriguez Gallegos, C. D.; Sofia, S. E.; Buonassisi, T. The Value of Efficiency in Photovoltaics. *Joule* **2019**, *3* (11), 2732–2747. <https://doi.org/10.1016/j.joule.2019.07.028>.
- (36) Mali, S. S.; Kim, H.; Patil, J. V.; Hong, C. K. Bio-Inspired Carbon Hole Transporting Layer Derived from Aloe Vera Plant for Cost-Effective Fully Printable Mesoscopic Carbon Perovskite Solar Cells. *ACS Appl. Mater. Interfaces* **2018**, *10* (37), 31280–31290. <https://doi.org/10.1021/acsami.8b08383>.
- (37) Miettunen, K.; Etula, J.; Saukkonen, T.; Jouttijärvi, S.; Halme, J.; Romu, J.; Lund, P. Insights into Corrosion in Dye Solar Cells. *Prog. Photovoltaics Res. Appl.* **2015**, *23* (8), 1045–1056. <https://doi.org/10.1002/pip.2534>.
- (38) Miettunen, K.; Vapaavuori, J.; Poskela, A.; Tiihonen, A.; Lund, P. D. Recent Progress in Flexible Dye Solar Cells. *Wiley Interdiscip. Rev. Energy Environ.* **2018**, *7* (5), e302. <https://doi.org/10.1002/wene.302>.
- (39) Miettunen, K.; Saukkonen, T.; Li, X.; Law, C.; Sheng, Y. K.; Halme, J.; Tiihonen, A.; Barnes, P. R. F.; Ghaddar, T.; Asghar, J.; Lund, P.; O'Regan, B. C. Do Counter Electrodes on Metal Substrates Work with Cobalt Complex Based Electrolyte in Dye Sensitized Solar Cells? *J. Electrochem. Soc.* **2012**, *160* (2), H132–H137. <https://doi.org/10.1149/2.074302jes>.
- (40) Wikberg, H.; Grönqvist, S.; Niemi, P.; Mikkelsen, A.; Siika-aho, M.; Kanerva, H.; Käsper, A.; Tamminen, T. Hydrothermal Treatment Followed by Enzymatic Hydrolysis and Hydrothermal Carbonization as Means to Valorise Agro- and Forest-Based Biomass Residues. *Bioresour. Technol.* **2017**, *235*, 70–78. <https://doi.org/10.1016/j.biortech.2017.03.095>.
- (41) Poskela, A.; Miettunen, K.; Borghei, M.; Vapaavuori, J.; Greca, L. G.; Lehtonen, J.; Solin, K.; Ago,

M.; Lund, P. D.; Rojas, O. J. Nanocellulose and Nanochitin Cryogels Improve the Efficiency of Dye Solar Cells. *ACS Sustain. Chem. Eng.* **2019**, *7* (12), 10257–10265.

<https://doi.org/10.1021/acssuschemeng.8b06501>.

- (42) Brunauer, S.; Emmett, P. H.; Teller, E. Adsorption of Gases in Multimolecular Layers. *J. Am. Chem. Soc.* **1938**, *60*, 309.
- (43) Lastoskie, C.; Gubbins, K. E.; Quirke, N. Pore Size Heterogeneity and the Carbon Slit Pore: A Density Functional Theory Model. *Langmuir* **1993**, *9* (10), 2693–2702.  
<https://doi.org/10.1021/la00034a032>.
- (44) Tiihonen, A.; Miettunen, K.; Halme, J.; Lepikko, S.; Poskela, A.; Lund, P. D. Critical Analysis on the Quality of Stability Studies of Perovskite and Dye Solar Cells. *Energy Environ. Sci.* **2018**, *11* (4).  
<https://doi.org/10.1039/c7ee02670f>.
- (45) Poskela, A.; Miettunen, K.; Tiihonen, A.; Lund, P. D. The State of External Circuit Affects the Stability of Dye-Sensitized Solar Cells. *Electrochim. Acta* **2018**, 275.  
<https://doi.org/10.1016/j.electacta.2018.04.117>.
- (46) Asghar, M. I.; Miettunen, K.; Mastroianni, S.; Halme, J.; Vahlman, H.; Lund, P. In Situ Image Processing Method to Investigate Performance and Stability of Dye Solar Cells. *Sol. Energy* **2012**, *86* (1). <https://doi.org/10.1016/j.solener.2011.10.006>.
- (47) Kinney, T. J.; Masiello, C. A.; Dugan, B.; Hockaday, W. C.; Dean, M. R.; Zygourakis, K.; Barnes, R. T. Hydrologic Properties of Biochars Produced at Different Temperatures. *Biomass and Bioenergy* **2012**, *41*, 34–43. <https://doi.org/10.1016/j.biombioe.2012.01.033>.
- (48) Labbé, N.; Harper, D.; Rials, T.; Elder, T. Chemical Structure of Wood Charcoal by Infrared Spectroscopy and Multivariate Analysis. *J. Agric. Food Chem.* **2006**, *54* (10), 3492–3497.

<https://doi.org/10.1021/jf053062n>.

- (49) Keiluweit, M.; Nico, P. S.; Johnson, M. G.; Kleber, M. Dynamic Molecular Structure of Plant Biomass-Derived Black Carbon (Biochar). *Environ. Sci. Technol.* **2010**, *44* (4), 1247–1253. <https://doi.org/10.1021/es9031419>.
- (50) Miettunen, K.; Toivola, M.; Hashmi, G.; Salpakari, J.; Asghar, I.; Lund, P. A Carbon Gel Catalyst Layer for the Roll-to-Roll Production of Dye Solar Cells. *Carbon N. Y.* **2011**, *49* (2), 528–532. <https://doi.org/10.1016/j.carbon.2010.09.052>.
- (51) Hashmi, S. G.; Halme, J.; Saukkonen, T.; Rautama, E.-L.; Lund, P. High Performance Low Temperature Carbon Composite Catalysts for Flexible Dye Sensitized Solar Cells. *Phys. Chem. Chem. Phys.* **2013**, *15* (40), 17689. <https://doi.org/10.1039/c3cp52982g>.
- (52) Halme, J.; Vahermaa, P.; Miettunen, K.; Lund, P. Device Physics of Dye Solar Cells. *Advanced Materials*. John Wiley & Sons, Ltd September 15, 2010, pp E210–E234. <https://doi.org/10.1002/adma.201000726>.
- (53) Mastroianni, S.; Asghar, I.; Miettunen, K.; Halme, J.; Lanuti, A.; Brown, T. M.; Lund, P. Effect of Electrolyte Bleaching on the Stability and Performance of Dye Solar Cells. *Phys. Chem. Chem. Phys.* **2014**, *16* (13). <https://doi.org/10.1039/c3cp55342f>.
- (54) Andrade, M. A. S.; Miettunen, K.; Tiihonen, A.; Lund, P. D.; Nogueira, A. F.; Pastore, H. O. Stabilizing Dendron-Modified Talc-Based Electrolyte for Quasi-Solid Dye-Sensitized Solar Cell. *Electrochim. Acta* **2017**, *228*, 413–421. <https://doi.org/10.1016/j.electacta.2017.01.101>.

Figure 1. Process from brewery residues to dye solar cells with activated biocarbon counter electrodes.

Figure 2 FTIR spectra of the produced biocarbons illustrates the effects of material treatments in the surface activity of the biocarbon material. Activation treatment after the heat treatment increases surface activity of the material.

Figure 3 SEM image of the biocarbon based counter electrode shows the highly porous structure of the material.

Figure 4. Initial JV curves of the solar cells with biocarbon (8 cells) and reference material Pt (8 cells) as counter electrode catalysts.

Figure 5: a) Short circuit current density  $J_{sc}$ , b) open circuit voltage  $V_{oc}$ , c) fill factor FF, and d) efficiency  $\eta$  of the Pt (P) and biocarbon (B) devices during extended aging test under 1Sun visible light illumination. In total 8 and 7 devices are shown for biocarbon and Pt devices, respectively (one Pt device was dropped from the graph because of a poor electrical connection to the potentiostat).  $J_{sc}$  and  $\eta$  data has been scaled to remove the effects of stray light that arises from aging the devices without any mask (raw data is presented in supplementary material). Two cutoffs in the data are caused by a data collection error. The data has been measured in aging test setup with closely monitored environmental conditions but the calibration is not as accurate as in a AAA solar simulator.

Figure 6: Incident photon to current efficiency (IPCE) of Pt (P) and biocarbon dye solar cells (B) a) before the aging, b) before the aging normalized by the maximum value of each curve, c) after the aging d) after the aging normalized by the maximum value of each curve. Biocarbon devices have higher IPCE than the reference Pt solar cells both before and after the aging test.

Figure 7:  $J_{sc}$  as a function of light intensity a) before and b) after the aging test as well as c) after the aging test normalized with the curves of the fresh devices for the individual cells. Biocarbon solar cells (B) show stable or improved performance after the aging test whereas the reference Pt solar cells (P) show suppressed limiting current density at light intensities starting from 2Sun after the aging test.

Table 1 Surface area, porosities, and elemental composition of the produced biocarbons.

Treatment stage	Precursor biocarbon	Heat treatment	Activation treatment
Activation yield/%	-	45	28
Surface area/m <sup>2</sup> g <sup>-1</sup>	5.2	15	2190
Total pore volume/ cm <sup>3</sup> g <sup>-1</sup>	-	0.007	0.857
Micropores/%	-	84.4	78.4
Mesopores/%	-	15.2	15.3
Macropores/%	-	0.4	6.3
C/wt-%	69	85	92
H/wt-%	6.7	0.6	0.6
N/wt-%	3.8	3.8	1.4
S/wt-%	0.12	0.05	0.06
O/wt-%	15	3.5	7.5

Table 2. Performance of devices before and after 3000 h aging under visible-only illumination when using the Pt and biocarbon catalysts.

	Pt	Biocarbon

<b>Before aging</b>		
$J_{sc}/\text{mA cm}^{-2}$	$10.6 \pm 0.3$	$10.5 \pm 0.5$
$V_{oc}/\text{mV}$	$785 \pm 8$	$676 \pm 37$
FF/%	$63 \pm 2$	$51 \pm 2$
$\eta/\%$	$5.3 \pm 0.2$	$3.6 \pm 0.2$
$R_s/\text{Ohm}$	$39 \pm 4$	$52 \pm 9$
# of devices	8	8
<b>After aging</b>		
$J_{sc}/\text{mA cm}^{-2}$	$11.4 \pm 0.5$	$11.4 \pm 0.5$
$V_{oc}/\text{mV}$	$690 \pm 4$	$584 \pm 43$
FF/%	$56 \pm 5$	$38 \pm 5$
$\eta/\%$	$4.4 \pm 0.6$	$2.5 \pm 0.3$
$R_s/\text{Ohm}$	$36 \pm 6$	$109 \pm 47$
# of devices	8	8